

Article

# Development of Representative Sailing Mode Construction Methodology Using Markov Chain

Changjae Moon <sup>1</sup>, Sanghun Jeong <sup>2</sup>, Giltae Roh <sup>1</sup> and Kido Park <sup>1,\*</sup>

<sup>1</sup> R&D Center, Korean Register, Busan 46762, Republic of Korea; cjmoon@krs.co.kr (C.M.); gtroh@krs.co.kr (G.R.)  
<sup>2</sup> Department of Statistics, Pusan National University, Busan 46241, Republic of Korea; shjeong95@pusan.ac.kr  
\* Correspondence: kdpark@krs.co.kr

**Abstract:** The strengthening of regulations such as EEXI, EEDI, and CII on ship emissions is underway. Despite their application, objective comparisons of ships are hindered by diverse navigation patterns and varying velocity regulations in different seas and ports. Additionally, a lack of basic data impedes comparisons of the optimal design and objective energy efficiency for ships. To address these issues, representative sailing modes, similar to those in the automobile industry, are needed. However, there is no reference for marine applications. This study introduces a methodology for representative sailing modes using the Markov chain. A hundred candidate sailing modes were created, and representative modes were identified through an evaluation equation. All chi-square values for representative sailing modes are within 1%, indicating significant results. This study's findings can aid in designing optimized systems for new vessels and computing authorized fuel efficiency for vessels with diverse sailing patterns.

**Keywords:** navigation pattern; mode construction methodology; sailing mode; ship design; fuel efficiency; representative



**Citation:** Moon, C.; Jeong, S.; Roh, G.; Park, K. Development of Representative Sailing Mode Construction Methodology Using Markov Chain. *J. Mar. Sci. Eng.* **2024**, *12*, 329. <https://doi.org/10.3390/jmse12020329>

Academic Editor: Burak Can Cerik

Received: 5 January 2024

Revised: 8 February 2024

Accepted: 8 February 2024

Published: 14 February 2024



**Copyright:** © 2024 by the authors. Licensee MDPI, Basel, Switzerland. This article is an open access article distributed under the terms and conditions of the Creative Commons Attribution (CC BY) license (<https://creativecommons.org/licenses/by/4.0/>).

## 1. Introduction

In line with the objectives outlined in the UN's Climate Change Framework Convention and the Kyoto Protocol, the International Maritime Organization (IMO) has implemented a rule aimed at mitigating air pollution arising from ship emissions. This initiative incorporates Annex VI into the MARPOL 73/78 Convention [1]. The challenge faced by shipowners and operators in adhering to these new regulations necessitates the development of policies, strategies, and technical solutions [2–4].

The amendments to MARPOL Annex VI were ratified during the 76th session of the Marine Environment Protection Committee in June 2021 at the IMO. Consequently, vessels with a gross tonnage (G.T) of 400 and above engaged in oversea voyages are mandated to comply with the existing energy efficiency ship index (EEXI) to mitigate their greenhouse gas emissions. The IMO identifies applications such as EEDI and CII [5,6].

Despite their implementation, objectively comparing ships with the same energy efficiency index (EEDI), energy efficiency existing ship index (EEXI), and carbon intensity indicator (CII) remains challenging due to variations in the captain's navigation habits, navigation patterns by route and port environments, and diverse speed controls in different seas. This implies that even when two ships with different propulsion systems share the same EEXI, EEDI, and CII, their performance cannot be considered equal in identical sailing profiles. The energy efficiency of a ship varies depending on the sailing profile of the ship. For instance, assuming a ship with an engine propulsion system and another with an electric propulsion system operate under the same sailing profile with a 70–80% high load factor, the energy efficiency of the ship with the engine propulsion system surpasses that of the electric propulsion system [7,8].

To address this limitation, an authorized fuel efficiency measurement system has been proposed for use in the automobile industry [9], but it lacks references applicable to the marine

field. The driving modes of this system are based on the federal test procedure (FTP-75) and highway fuel economy test (HWFET), as depicted in Figures 1 and 2 [10–12]. The FTP-75 and HWFET, rearranged with the five driving cycle correction formula, are also utilized in South Korea [13]. The FTP-75, a city driving cycle derived from real driving profiles in Los Angeles [14], comprises numerous stop-and-go patterns [11,12]. The HWFET is a highway driving cycle [15] used to measure authorized fuel efficiency related to a highway driving pattern [16]. The five driving cycle calibrates the FTP-75 mode and HWFET mode. The Cold FTP-75 is a city driving cycle in low-temperature conditions, the US06 is the driving cycle with the fastest acceleration and deceleration, and the SC03 is a driving cycle with air conditioning [10,13].

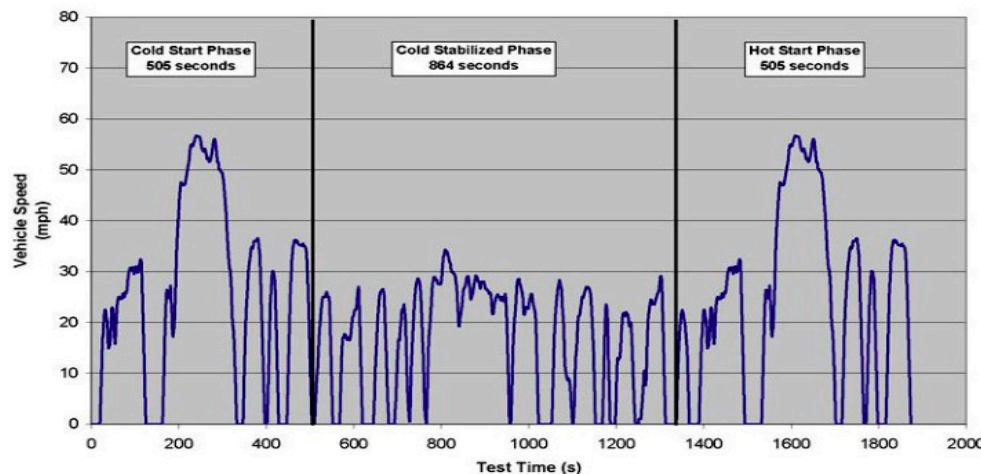


Figure 1. Graph of the FTP-75 mode [10].

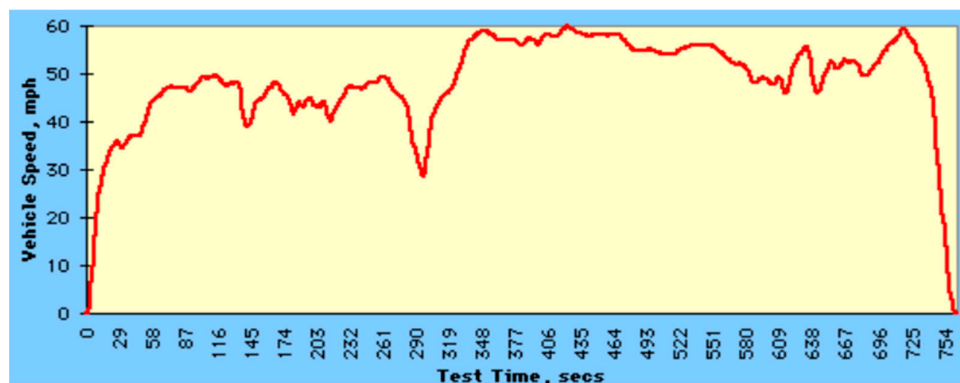


Figure 2. Graph of the HWFET mode [12].

Distinct driving modes have been developed in the automobile industry for city and highway driving since the 1970s to advance driving system development [17]. Authorized driving modes have significantly improved, with various methods being proposed in domestic and international studies, including an analysis of actual road driving patterns and the reconstruction of speed distribution [18], driving mode generation based on the definition of modal events such as acceleration and deceleration probability [19], and the use of conventional methods employing micro-trips [20,21]. However, directly applying these results to ships is challenging due to operational condition differences. Furthermore, the lack of data in marine industries makes it difficult to establish reliable representative sailing modes.

This study aims to create representative sailing modes based on probability. The initial step involves obtaining sailing profiles for a comparable ship type, sailing route, and y-axis value. Subsequently, the collected sailing profiles, including the selected ship type and sailing route (area), and the y-axis value undergo preprocessing. Based on specific criteria, hollow sailing

modes are derived from these sailing profiles. Raw sailing modes are segmented, and the transition probability matrix is calculated using the definition of modal events. Two methods, based on the number of sailing profiles, continuously generate segments using the Markov chain Monte Carlo algorithm. To validate this methodology, 100 candidate sailing modes were generated, and the representative sailing mode was selected among them using an evaluation equation. Finally, the representative sailing mode, applicable to ships with different outputs, is calculated, considering the diverse tonnages of each ship.

## 2. Methodology

Figure 3 illustrates the methodology for constructing modal event sailing modes; the methodology is divided into two distinct steps. In the initial phase, the objective of creating sailing modes is defined, whether for fuel efficiency measurement or ship design. Importantly, in contrast to automobiles, ships (hotel loads) commonly feature different propulsion outputs and load patterns, necessitating the meticulous determination of the y-axis value for speed or power. Subsequently, sailing profiles, incorporating the chosen ship type, sailing route (area), and y-axis value “y”, are compiled.

These profiles undergo preprocessing, culminating in the derivation of hollow sailing modes. Hollow sailing modes serve as the criterion for segregating the collected sailing profiles. Essentially, they play a pivotal role in generating raw sailing modes [22]. Furthermore, the gathered sailing profiles undergo normalization, transforming them into unit-gathered sailing profiles by dividing the y-axis by the maximum design “y” of the collected sailing profiles. These unit-gathered sailing profiles are categorized based on the hollow sailing modes obtained in the initial step. The unit-gathered sailing profiles, once classified, constitute raw sailing modes; then, segments are created by dividing the raw sailing modes into smaller components.

A segment, as depicted in Figure 4, represents the fundamental unit of a raw sailing mode, further divided into smaller pieces.  $t_{s0}$  represents the initial time of the segment,  $y_{s0}$  represents the initial y-axis value “y”,  $t_{sl}$  represents the last time of the segment, and  $y_{sl}$  denotes the y-axis value “y” of the segment at the end time. These segments possess unique characteristics, including average value and slope value. Through utilizing these factors, probabilities can be calculated, and random sampling can be undertaken.

Segments with either uniform or random time intervals can be generated, with each exhibiting distinct modal events within the raw sailing modes. The various types and definitions of these modal events are detailed in Table 1 and illustrated in Figure 5. Modal events encompass categories such as idle, cruise, acceleration, deceleration, divisions of acceleration, and divisions of deceleration. Notably, the divisions of acceleration and deceleration can be employed as alternatives to the broader categories of acceleration and deceleration.

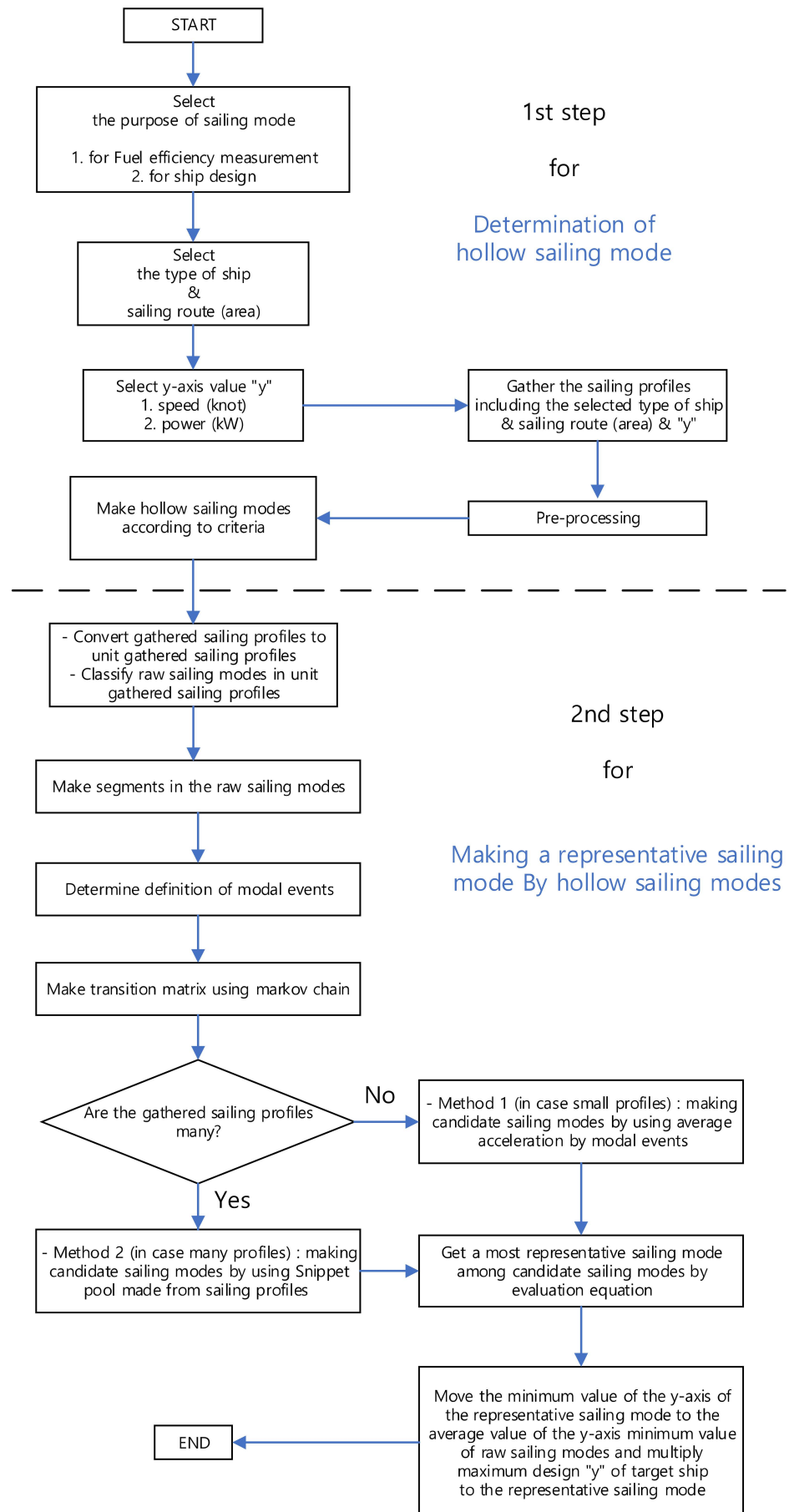


Figure 3. Methodology [22].

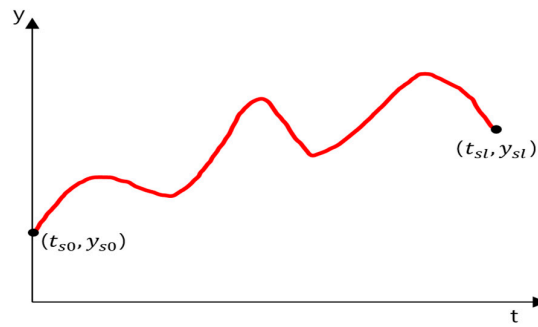


Figure 4. A segment chipped from the raw sailing modes.

Table 1. Definition of the modal events.

Modal Event	Definition
idle	$y_s^1$ s are below $k_1^2$ steadily
cruise	$y_s$ s are above $k_1$ steadily
acceleration	slope angle range( $k_2^3 \sim s_{max}^5$ )
deceleration	slope angle range( $k_3^4 \sim s_{min}^6$ )
accel-d-1	1st division of slope angle range( $k_2 \sim s_{max}$ ) divided by d ( $n \leq d$ )
accel-d-2	2nd division of slope angle range( $k_2 \sim s_{max}$ ) divided by d ( $n \leq d$ )
...	...
accel-d-n	n-th division of slope angle range( $k_2 \sim s_{max}$ ) divided by d ( $n \leq d$ )
decel-d-1	1st division of slope angle range( $k_3 \sim s_{min}$ ) divided by d ( $n \leq d$ )
decel-d-2	2nd division of slope angle range( $k_3 \sim s_{min}$ ) divided by d ( $n \leq d$ )
...	...
decel-d-n	n-th division of slope angle range( $k_3 \sim s_{min}$ ) divided by d ( $n \leq d$ )

<sup>1</sup> The y-axis value of a segment, which can either be speed (knot) or power (kW); <sup>2</sup> The constant velocity for cruise; <sup>3</sup> The positive constant close to 0°; <sup>4</sup> The negative constant close to 0°; <sup>5</sup> The average of the maximum slopes in the segments by the raw sailing modes; <sup>6</sup> The average of the minimum slopes in the segments by the raw sailing modes.

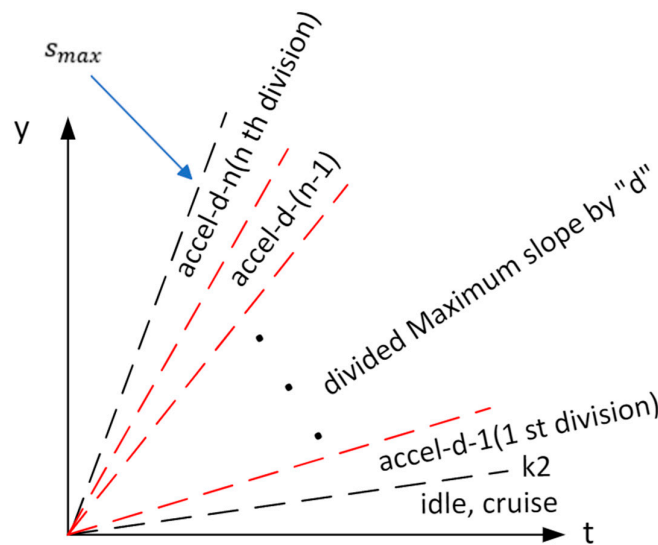


Figure 5. Divisions of the modal event “accel-d-n”.

The modal events are defined as shown in Table 2, which presents formulas for the modal events. The parameters presented in Table 2 can be obtained from the footnotes of Table 1.

**Table 2.** Formulas based on the modal events.

Modal Event	Formulas
idle	$k_3 < \frac{y_{sl}-y_{s0}}{t_{sl}-t_{s0}} < k_2$ and $y_{sm}^1 < k_1$
cruise	$k_3 < \frac{y_{sl}-y_{s0}}{t_{sl}-t_{s0}} < k_2$ and $y_{sm}^1 > k_1$
acceleration	$\frac{y_{sl}-y_{s0}}{t_{sl}-t_{s0}} > k_2$
deceleration	$\frac{y_{sl}-y_{s0}}{t_{sl}-t_{s0}} < k_3$
accel-d-1	$\frac{y_{sl}-y_{s0}}{t_{sl}-t_{s0}} > k_2$ and $k_2 \sim k_2 + 1 \times \frac{s_{max}-k_2}{d}$
accel-d-2	$\frac{y_{sl}-y_{s0}}{t_{sl}-t_{s0}} > k_2$ and $k_2 + 1 \times \frac{s_{max}-k_2}{d} \sim k_2 + 2 \times \frac{s_{max}-k_2}{d}$
...	...
accel-d-n	$\frac{y_{sl}-y_{s0}}{t_{sl}-t_{s0}} > k_2$ and $k_2 + (n-1) \times \frac{s_{max}-k_2}{d} \sim k_2 + n \times \frac{s_{max}-k_2}{d}$
decel-d-1	$\frac{y_{sl}-y_{s0}}{t_{sl}-t_{s0}} < k_3$ and $k_3 \sim k_3 + 1 \times \frac{s_{min}-k_3}{d}$
decel-d-2	$\frac{y_{sl}-y_{s0}}{t_{sl}-t_{s0}} < k_3$ and $k_3 + 1 \times \frac{s_{min}-k_3}{d} \sim k_3 + 2 \times \frac{s_{min}-k_3}{d}$
...	...
decel-d-n	$\frac{y_{sl}-y_{s0}}{t_{sl}-t_{s0}} < k_3$ and $k_3 + (n-1) \times \frac{s_{min}-k_3}{d} \sim k_3 + n \times \frac{s_{min}-k_3}{d}$

<sup>1</sup> Average of the y-axis value “y” in a segment.

Based on these modal events, a transition matrix is created using a Markov chain [23]. For the Markov process, the probability of states can be expressed as Equation (1):

$$P(P(X_0, X_1, \dots, X_T) = P(X_0) \prod_t P(X_t | X_{t-1}). \tag{1}$$

where X represents a sequence of random variables and t represents time. The Markov process is characterized by the determination of future states being unaffected by past states, allowing snippets to continue in the variation of data. It is suitable for making representative sailing modes using the Markov chain Monte Carlo algorithm when developing the representative sailing mode based on probability [22,24]. After selecting the modal event, the subsequent procedure follows two methods contingent on the number of gathered sailing profiles. Method 1 is employed when the number of gathered sailing profiles is limited. The essence of this method lies in generating candidate sailing modes using the average acceleration based on the modal events. Modal events are continuously generated based on the transition matrix to create candidate sailing modes. The initial input values for the candidate sailing modes are the average initial values of the raw sailing modes. The initial modal event of the candidate sailing mode is randomly selected. The snippet generation persists for the average duration of the raw sailing modes.

Method 2 is utilized when the number of gathered sailing profiles is substantial. The focus here is on generating candidate sailing modes using a snippet pool derived from the raw sailing modes. The snippet, as depicted in Figure 6, represents a processed segment. To seamlessly connect the end-point of the previous snippet to the starting point of the next snippet, the starting point of the segment is shifted to zero on the y-axis. Similar to Method 1, modal events are continuously generated based on the transition matrix.

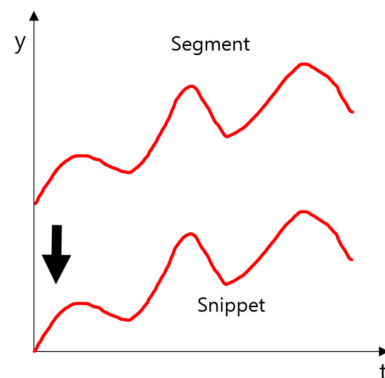


**Figure 6.** A snippet representing a processed segment.

In contrast to Method 1, Method 2 involves two additional stages for obtaining the candidate sailing modes after sampling the modal event from the transition matrix. One of these stages involves selecting either Group A or B. Table 3 outlines the formulas associated with the criteria for the selection of Groups A or B. If the difference between the average snippet and the initial value of the snippet was greater than zero, Group A was assigned; otherwise, Group B was selected.

**Table 3.** Formulas related to the criteria for selecting Group A or B.

Snippet Group	Formulas
Group A	$\frac{\int_{t_{s0}}^{t_{sl}} y_s(t) dt}{t_{sl} - t_{s0}} - y_{s0} > 0$
Group B	$\frac{\int_{t_{s0}}^{t_{sl}} y_s(t) dt}{t_{sl} - t_{s0}} - y_{s0} < 0$

After selecting Group A or B, a snippet was sampled in the residual m group. The residual R shown in Figure 7 represents the sum of the square of the difference between the “y” value of the snippet and that of slope line A.

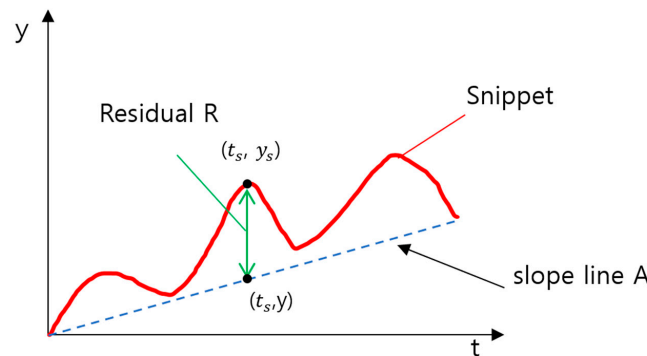


**Figure 7.** Residual R and slope line A.

Equation (2) depicts the residual R, where  $y_s$  represents the y-axis value of the snippet, and  $t_s$  represents the x-axis value of the snippet. Equation (3) outlines the slope line A, where y represents the y-axis value of slope line A, and t represents the x-axis value of slope line A. Figure 8 details the residual m group. Equation (4) describes the residual m group, where m represents a division,  $R_{min}$  represents the minimum of the residual R of the snippets, and  $R_{max}$  represents the maximum of the residual R of the snippets. Figure 9 illustrates the modal events and snippets in groups during the ocean-going mode.

$$R = \sum \left( y_s - \frac{y_{sl} - y_{s0}}{t_{sl} - t_{s0}} \times t_s \right)^2 \tag{2}$$

$$y = \frac{y_{sl} - y_{s0}}{t_{sl} - t_{s0}} \times t \tag{3}$$

$$n - \text{th of Residual m Group} = R_{min} + \frac{R_{max} - R_{min}}{m} \times (n - 1) \sim R_{min} + \frac{R_{max} - R_{min}}{m} \times n \tag{4}$$

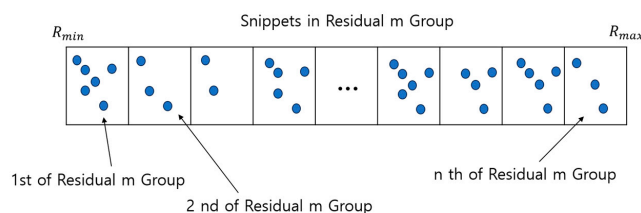


**Figure 8.** Residual m group in the snippet A Group.

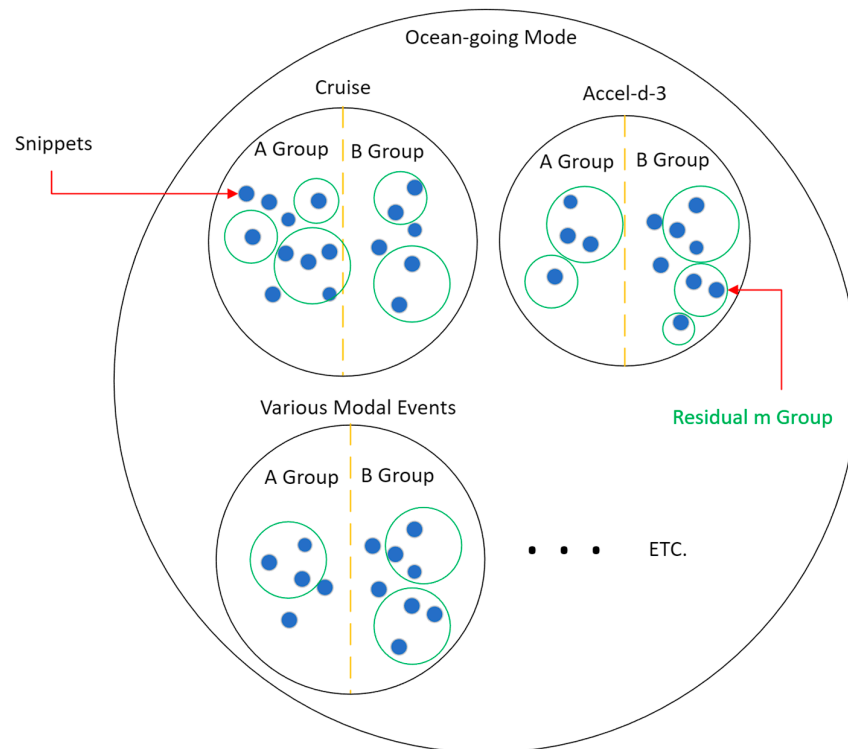


**Figure 9.** Example of the modal events and snippets in groups during the Ocean-going mode.

After creating candidate sailing modes using Method 2, post-processing is required, as shown in Figure 10. The excess sharp points in the original candidate sailing mode are shifted to the maximum sharp point, which is the sharpest point among the raw sailing modes.

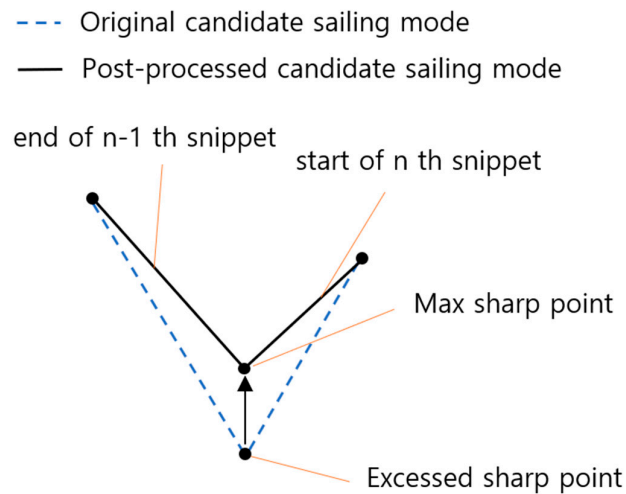


**Figure 10.** Post-processing.

Snippet sampling for creating candidate sailing modes varies depending on whether the representative sailing mode is intended for ship design or fuel efficiency measurements. In the case of ship design, the number of snippets generated equals the average total time of the raw sailing modes. For fuel efficiency measurements, users have the flexibility to create as many snippets as needed.

Equation (5) is utilized to calculate the representative sailing mode from the candidate sailing modes created by Methods 1 or 2. The candidate sailing mode with the smallest  $Y_{rep}$  is the representative sailing mode. The  $z$  score, expressed in Equation (6), represents

a standard normal distribution, and the square of the Z-score, as illustrated in Figure 11 and Equation (5), is a chi-square distribution. The choice of a chi-square distribution is justified due to the essential standardization, given the varying range of evaluation values in the representative sailing modes. Moreover, to integrate these standardized values into one measure, it was deemed most appropriate to transform them into values of chi-square distribution based on mathematical statistics. Here, “m” denotes the number of raw sailing modes, RMSE signifies the root mean square error between the candidate sailing mode and raw sailing modes, “y” denotes the speed or power determined in step 1,  $y_{avg.c}$  is the average of “y”s in candidate sailing mode  $y_{avg.r}$ , is the average of “y”s of raw sailing modes, SAFD denotes the speed–acceleration frequency distribution between the candidate sailing mode and raw sailing modes,  $R_c$  indicates the relative positive acceleration (RPA) of the candidate sailing mode, and  $R_r$  denotes the RPAs of the raw sailing modes.

$$Y_{rep} = \{zscore(\sum_{i=1}^m ((y_{avg.c} - y_{avg.ri})^2))\}^2 + \{zscore(\sum_{i=1}^m (R_c - R_{ri})^2)\}^2 + \{zscore(\sum_{i=1}^m (RMSE))\}^2 + \{zscore(\sum_{i=1}^m (SAFD)^2)\}^2 \sim \chi^2(4) \tag{5}$$

$$zscore(x_{(k)}) = \{x_{(k)} - mean(x)\} / sd(x) \tag{6}$$

zscore( $x_{(k)}$ ) : zscore of k – th sample of x – value  
sd : standard deviation of x

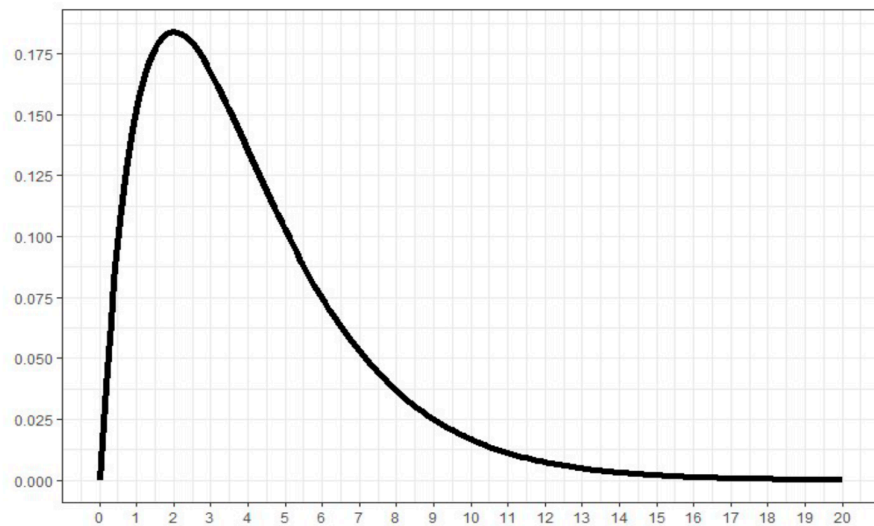


Figure 11. Chi-square distribution.

In the automobile sector, the abstraction of the candidate cycle SAFD and sample SAFD is utilized in the generation of driving modes [25,26].

This parameter is referred to as the “SAFDdiff.” The SAFD is expressed as Equation (7) [27]:

$$SAFD = \sum_a \sum_v |fr_{(a,v)} - p_{(a,v)}| \tag{7}$$

where  $fr_{(a,v)}$  is a frequency of snippets at speed v and acceleration a in the candidate sailing mode, and  $p_{(a,v)}$  denotes the frequency of snippets at speed v and acceleration a in the raw sailing modes. The RPA represents the load variation of a voyage [28]. This variation is expressed in Equation (8). Herein,  $a_i$  represents the acceleration at time I, and  $v_i$  denotes the velocity at time i.

$$RPA = \frac{1}{\int_1^n v_i dt} \sum_{i=1}^n a_i v_i (a_i > 0) \tag{8}$$

0 (else)

Finally, the representative sailing mode can be utilized by shifting the average of the minimum values of the raw sailing modes in the positive direction of the y-axis and multiplying the maximum design “y” of the target ship.

### 3. Selection of the Target for Generating the Representative Sailing Mode

#### 3.1. Target Ship and Voyages

The focus of this study is the “Hannara” ship affiliated with the Korea Maritime and Ocean University (KMOU) located in Busan, which is utilized for student training [29]. Three voyages were randomly selected from the sailing profiles: the KMOU–Masan–KMOU voyage, the KMOU–Ulleung–KMOU voyage, and the KMOU–Incheon–KMOU voyage. Comprehensive details regarding the KMOU–Masan–KMOU voyage are available in Table 4, with visual representations being presented in Figures 12 and 13. Figure 14 further illustrates the profiles of the KMOU–Masan–KMOU voyage.

**Table 4.** Voyage record for the KMOU–Masan–KMOU voyage.

Voyage Record		
1 November 2021	10:36 Stand by in KMOU 11:42 Ocean going from KMOU	Stand by 1.1 h
2 November 2021	09:30 Stand by at Masan 12:42 Engine stop	Sailing 21.8 h Stand by 3.2 h
3 November 2021	09:36 Stand by in Masan 11:12 Ocean going to KMOU	Stand by 1.6 h
4 November 2021	09:00 Stand by at KMOU 10:36 Engine stop	Sailing 21.8 h Stand by 1.6 h

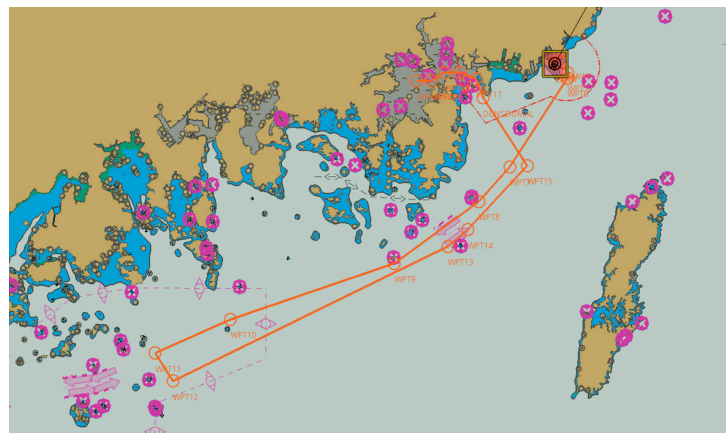


**Figure 12.** Voyage from KMOU to Masan.

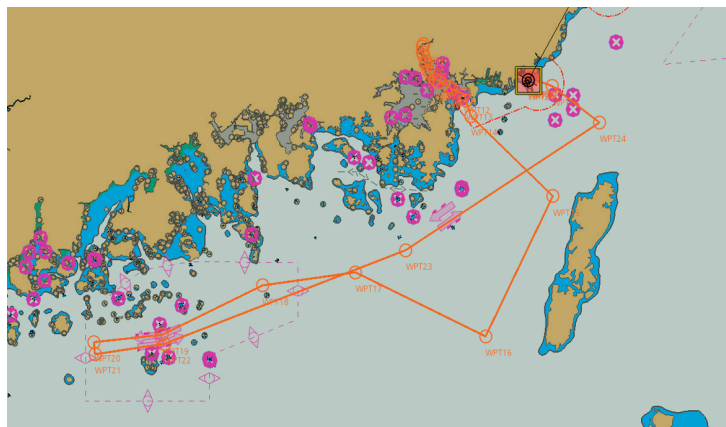


**Figure 13.** Voyage from Masan to KMOU.

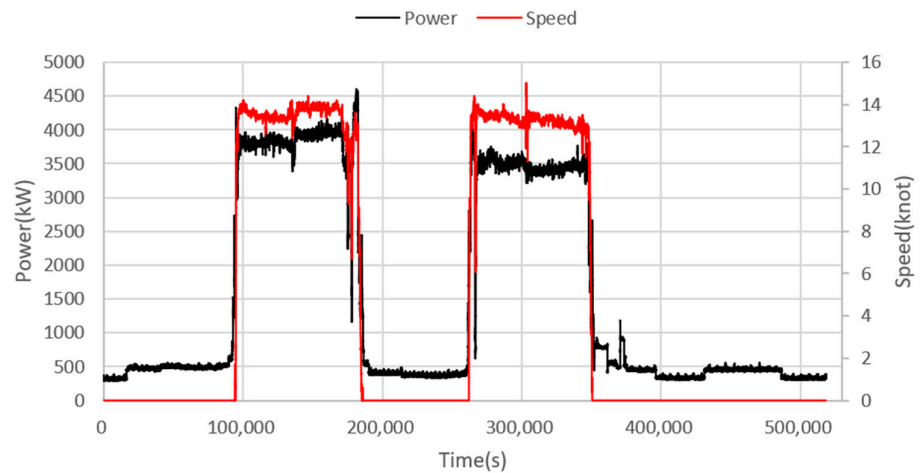


Figure 14. Graph of the KMOU–Masan–KMOU voyage.

Detailed information regarding the KMOU–Ulleung–KMOU voyage is presented in Table 5 and Figures 15 and 16. Figure 17 shows the profiles of the KMOU–Ulleung–MOU voyage.

Table 5. Voyage record for the KMOU–Ulleung–KMOU voyage.

Voyage Record		
25 June 2022	12:54 Stand by in KMOU 13:30 Ocean going from KMOU	Stand by 0.6 h
26 June 2022	08:30 Stand by at Ulleung 10:00 Engine stop	Sailing 19.0 h Stand by 1.5 h
27 June 2022	15:42 Stand by Eng for Dep. from Ulleung 16:06 Ocean going to KMOU	Stand by 0.4 h
28 June 2022	06:00 Stand by at KMOU 07:30 Engine stop	Sailing 13.9 h Stand by 1.5 h

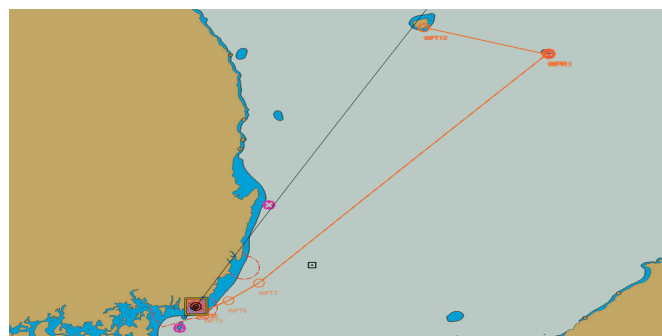


Figure 15. Voyage from KMOU to Ulleung.



Figure 16. Voyage from Ulleung to KMOU.

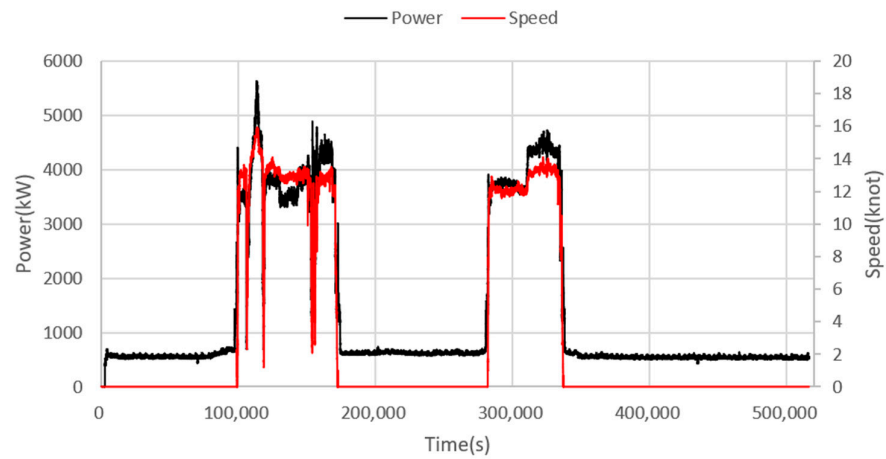


Figure 17. Graph of the KMOU–Ulleung–KMOU voyage.

Detailed information regarding the Busan–Incheon–Busan voyage is presented in Table 6 and Figures 18 and 19. Figure 20 shows the sailing profiles of the Busan–Incheon–Busan voyage.

Table 6. Voyage record for the KMOU–Incheon–KMOU voyage.

Voyage Record		
29 November 2021	10:06 Stand by in KMOU	Stand by 0.6 h
	10:42 Ocean going from KMOU	Sailing 26.8 h
30 November 2021	13:30 Stand by in Incheon	Stand by 0.8 h
	14:18 Engine stop	
1 December 2021	13:12 Stand by in Incheon	Stand by 0.6 h
	13:48 Ocean going from Incheon	Sailing 25.2 h
2 December 2021	15:00 Stand by in KMOU	Stand by 2.0 h
	17:00 Engine stop	

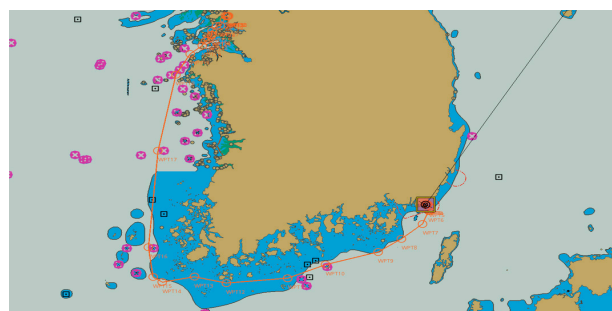


Figure 18. Voyage from KMOU to Incheon.



Figure 19. Voyage from Incheon to KMOU.

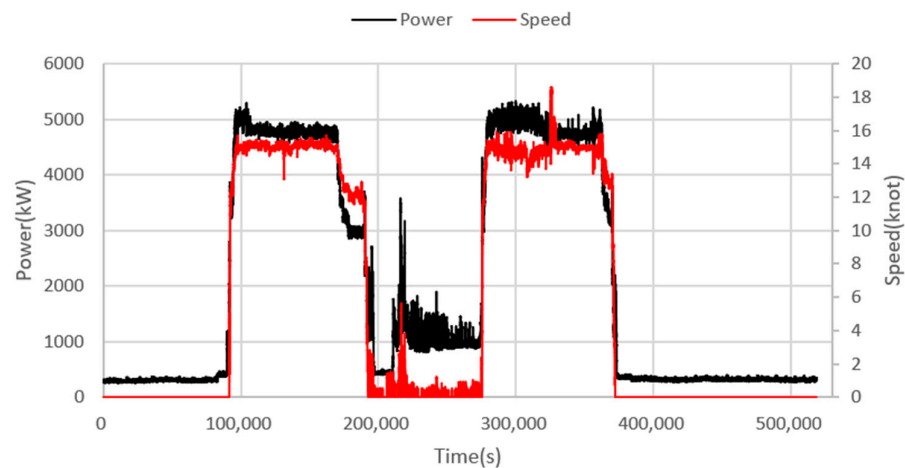


Figure 20. Graph of the KMOU–Incheon–KMOU voyage.

3.2. Prerequisites for the Generation of the Representative Sailing Mode

The prerequisites for creating a representative sailing mode are outlined in Table 7. The Y-axis values, denoted as “y,” may differ from the sailing modes depicted in Table 8. This discrepancy arises because, depending on the mode, there are instances where the ship velocity is zero, yet the generator output persists. To ensure a comprehensive assessment of fuel efficiency, we opted to generate one hundred snippets for the representative sailing mode.

Table 7. Prerequisites for generating the representative sailing mode.

Items	Contents
Mode purpose	Fuel efficiency measurement
Type of ship	Training ship
Sailing route	KMOU–Masan–KMOU, KMOU–Ulleung–KMOU, KMOU–Incheon–KMOU
Y-axis value “y”	Speed (knot) and power (kW)
Maximum design power	6618 kW
Maximum design speed	18.5 knot
“d” of the modal event	5
“m” of Residual m group	10
The number “k” of snippets based on the mode	100

Table 8. y-axis value “y” derived from using the sailing modes.

Sailing Modes	y-Axis Value “y”
Stand by mode	kW
Port out (v = 0) mode	kW
Port out mode	knot
Navigation mode	knot
Port in mode	knot
Port in (v = 0) mode	kW

4. Results

To validate the proposed methodology, we implemented codes using MATLAB programs, organized into m files, covering each detailed procedure outlined in Figure 21. The code structure comprises a main part and a verification part. The main part encompasses the classification of sailing modes from raw data in Excel files, the creation of result files, the division of raw data into snippets, state calculation based on snippets, the sampling of candidate sailing modes using the Markov chain Monte Carlo algorithm, and the calculation

of result values using the evaluation equation. The verification part includes the utilization of the chi-square test. Given the fuel efficiency measurement objective, 100 snippets were generated for each sailing mode, each spanning approximately 1 h. The computation times for the representative sailing modes are presented in Table 9. The selection of the representative sailing mode from the 100 candidates was accomplished using Equation (5).

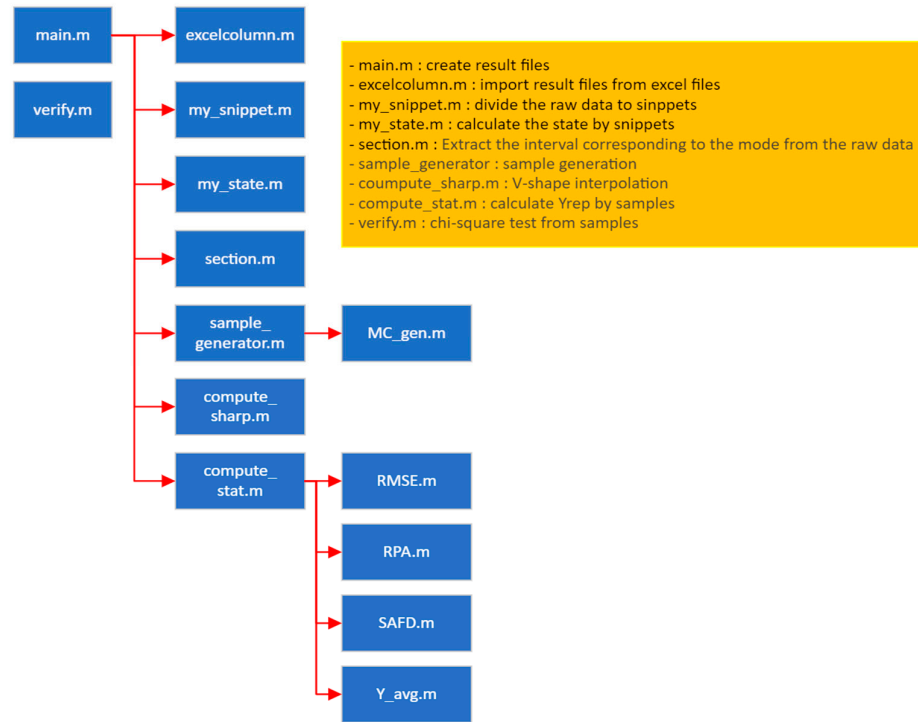


Figure 21. MATLAB 2023a (version 2023a, MathWorks company, Natick, MA, USA) m files configuration.

Table 9. Computation times of the representative sailing modes.

The Representative Sailing Mode	Computation Time(s)
Stand by mode	4130
Port out (v = 0) mode	4070
Port out mode	4110
Navigation mode	4030
Port in mode	3980
Port in (v = 0) mode	3970

The stand by mode among the representative sailing modes is depicted in Figure 22. In this mode, the training ship is in harbor, and only the generator operates. As the generator functions to supply necessary power at the port, no significant load change was observed. The unit total power ranged between 0.04 and −0.05, and the modal event exhibited consistency, as indicated in Table 10.

Table 10. Number of modal events in the stand by mode.

Modal Event	Number	Proportion(%)	Modal Event	Number	Proportion(%)
accel-5-1	58	11.3	decel-5-1	58	9.3
accel-5-2	61	11.9	decel-5-2	61	7.6
accel-5-3	59	11.5	decel-5-3	59	9.1
accel-5-4	59	11.5	decel-5-4	59	7.8
accel-5-5	56	10.9	decel-5-5	56	9

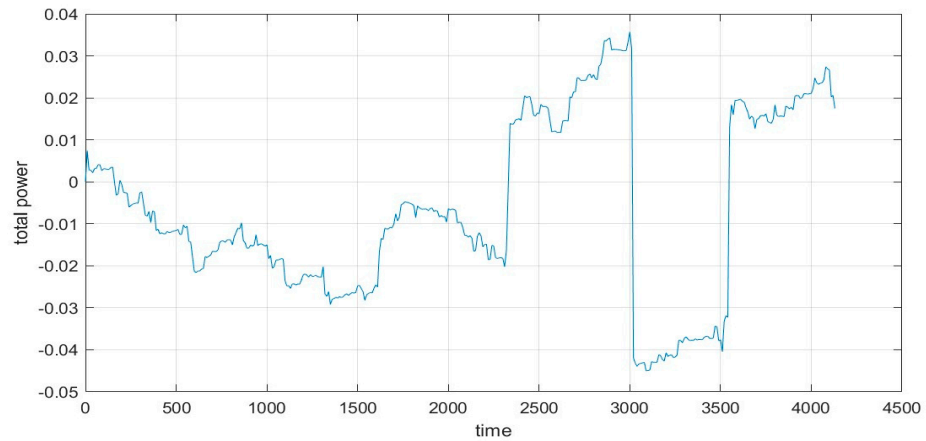


Figure 22. Stand by mode.

The port out ( $v = 0$ ) mode among the representative sailing modes is illustrated in Figure 23. Similar to the stand by mode, the ship is in harbor, and only the generator operates, but in this mode, the unit total power increases in preparation for departure. The unit total power ranged between 0 and 1.7, and there was a higher proportion for the acceleration part of the modal event compared to the deceleration part, as presented in Table 11.

Table 11. Number of modal events in the port out ( $v = 0$ ) mode.

Modal Event	Number	Proportion(%)	Modal Event	Number	Proportion(%)
accel-5-1	64	12.6	decel-5-1	35	6.9
accel-5-2	56	11	decel-5-2	40	7.9
accel-5-3	73	14.4	decel-5-3	29	5.7
accel-5-4	60	11.8	decel-5-4	45	8.9
accel-5-5	67	13.2	decel-5-5	38	7.5

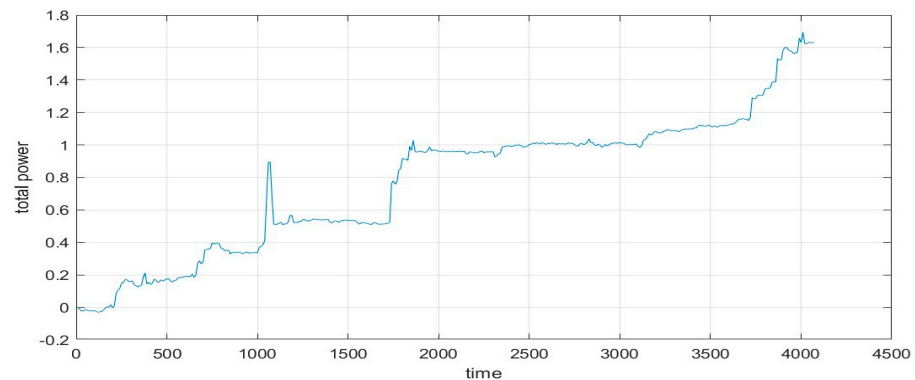
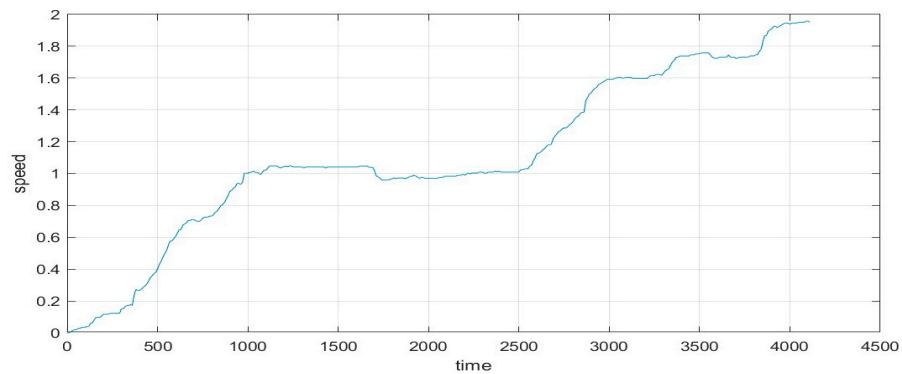


Figure 23. Port out ( $v = 0$ ) mode.

The port out mode among the representative sailing modes is displayed in Figure 24. In this mode, the training ship departs from the harbor, with both the generator and the engine operating. The unit total power ranged between 0 and 2, with there being an extremely higher proportion for the acceleration part of the modal event compared to the deceleration part, as shown in Table 12.

**Table 12.** Number of modal events in the port out mode.

Modal Event	Number	Proportion(%)	Modal Event	Number	Proportion(%)
accel-5-1	79	18.2	decel-5-1	10	2.3
accel-5-2	49	11.3	decel-5-2	16	3.7
accel-5-3	93	21.5	decel-5-3	12	2.8
accel-5-4	72	16.6	decel-5-4	13	3
accel-5-5	79	18.3	decel-5-5	9	2



**Figure 24.** Port out mode.

The navigation mode among the representative sailing modes is depicted in Figure 25. This mode occurs when the training ship navigates in the ocean. Unlike the port out mode, there was no significant speed change, as sailing vessels tend to maintain a constant speed. The unit total power ranged between  $-0.08$  and  $0.07$ , and the modal event exhibited consistency, as indicated in Table 13.

**Table 13.** Number of modal events in the navigation mode.

Modal Event	Number	Proportion(%)	Modal Event	Number	Proportion(%)
accel-5-1	20	6	decel-5-1	34	10.3
accel-5-2	42	12.8	decel-5-2	34	10.3
accel-5-3	31	9.4	decel-5-3	36	10.9
accel-5-4	29	8.8	decel-5-4	36	10.9
accel-5-5	32	9.7	decel-5-5	35	10.6

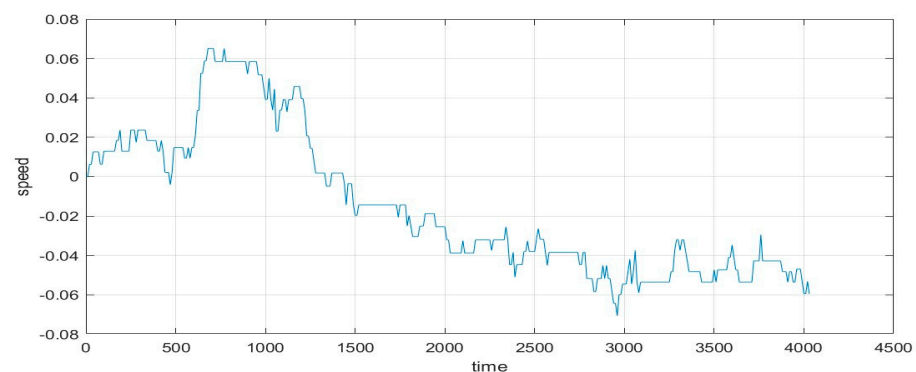


**Figure 25.** Navigation mode.

The port in mode among the representative sailing modes is shown in Figure 26. This mode occurs when the training ship enters the harbor, with both the generator and the engine operating. The unit total power ranged between 0 and  $-1.8$ , with there being a

significantly higher proportion for the deceleration part of the modal event compared to the acceleration part, as presented in Table 14.

**Table 14.** Number of modal events in the port in mode.

Modal Event	Number	Proportion(%)	Modal Event	Number	Proportion(%)
accel-5-1	13	3	decel-5-1	72	16.4
accel-5-2	22	5	decel-5-2	72	16.4
accel-5-3	14	3.2	decel-5-3	72	16.4
accel-5-4	14	3.2	decel-5-4	71	16.2
accel-5-5	21	4.8	decel-5-5	67	15.3

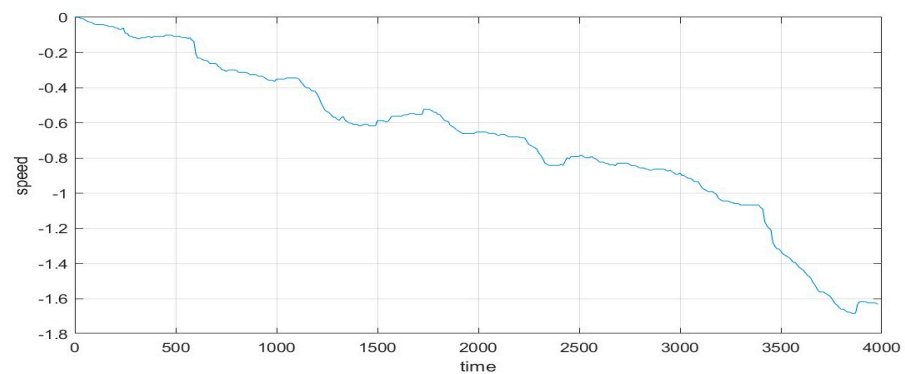


**Figure 26.** Port in mode.

The port in ( $v = 0$ ) mode among the representative sailing modes is illustrated in Figure 27. This mode occurs when the training ship is in the harbor and serves as an intermediate stage between the stand by mode and port in mode. Only the generator operates, and unlike the stand by mode, the unit total power decreases in preparation for anchoring. The unit total power ranged between 0 and  $-1.7$ , with there being a higher proportion of the deceleration part of the modal event compared to the acceleration part, as shown in Table 15.

**Table 15.** Number of modal events in the port in ( $v = 0$ ) mode.

Modal Event	Number	Proportion(%)	Modal Event	Number	Proportion(%)
accel-5-1	42	8.5	decel-5-1	54	10.9
accel-5-2	50	10	decel-5-2	52	10.5
accel-5-3	41	8.2	decel-5-3	52	10.5
accel-5-4	48	9.7	decel-5-4	50	10
accel-5-5	46	9.3	decel-5-5	62	12.5

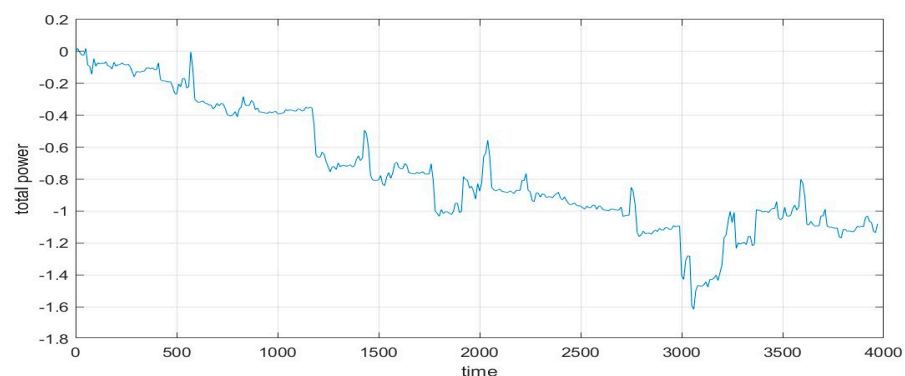


**Figure 27.** Port in ( $v = 0$ ) mode.

To validate the representative sailing modes, the chi-square test was employed. A chi-square value within the 5% threshold was utilized to determine the significance of the results [30]. All chi-square values corresponding to the representative sailing modes, as depicted in Table 16, were below 0.01, signifying significant results.

**Table 16.** Chi-square values corresponding to the sailing modes.

Sailing Modes	Chi-Square Value
Stand by mode	0.014
Port out (v = 0) mode	0.197
Port out mode	0.246
Navigation mode	0.188
Port in mode	0.032
Port in (v = 0) mode	0.074

### 5. Conclusions

This study devised a methodology for crafting a representative ship sailing mode by employing a Markov chain. Unlike the automobile industry, the shipbuilding and shipping sector lack the concept of a representative sailing mode. However, with the growing emphasis on eco-friendliness and economy, there is an escalating demand for a representative sailing mode in fuel efficiency measurement and the analysis of optimized ship designs. Particularly, given the potential disparities in system configurations among ships of the same type, a representative sailing mode becomes pivotal for precise comparisons. In ship design, the incorporation of a representative sailing mode facilitates an optimal design, fostering economically and ecologically friendly ship development. In this study, to validate the methodology, sailing profile data for Masan, Ulleung, and Incheon on the Hannara ship of the Korea Maritime University were acquired and segmented into small units known as snippets. Modal events were categorized by each snippet, leading to the creation of a probability transition matrix. Subsequently, an additional probability technique was applied to enhance representativeness, culminating in the derivation of the representative sailing mode using the chi-square calculation equation. The chi-square values associated with the resultant representative sailing modes were within 1%, signifying statistically meaningful outcomes. One limitation of our study is the somewhat constrained representativeness attributed to the limited dataset we used. Future studies should prioritize acquiring a more extensive dataset to derive a robust representative sailing mode and validate its significance through chi-square tests. Furthermore, further research on designing optimized systems for new vessels and computing the authorized fuel efficiency of vessels using representative sailing modes should be pursued in the future. By employing this methodology, users and the shipping community can pinpoint representative sailing modes for each ship type, comprehend sailing pattern trends, and assess their impact on fuel costs and carbon dioxide emissions. These data can serve as foundational information for developing innovative ship designs with new systems and can assist policymakers in calculating the environmental benefits associated with transitioning to eco-friendly propulsion systems.

**Author Contributions:** K.P.: funding acquisition, project administration, resources, conceptualization. S.J.: software, writing—review and editing. C.M.: formal analysis, investigation, methodology, validation, visualization, writing—original draft. G.R.: data curation, formal analysis, writing—review and editing. All authors have read and agreed to the published version of the manuscript.

**Funding:** This work was supported by the Technology Innovation Program (or Industrial Strategic Technology Development Program—Development of fuel cell system design and verification platform technology to hydrogen mobility) (00144182, Development of mobility driving mode for expansion of fuel cell system hybrid power system), funded By the Ministry of Trade, Industry & Energy (MOTIE, Korea). This research was supported by the Korea Institute of Marine Science & Technology Promotion (KIMST), funded by the Ministry of Oceans and Fisheries (20210369).

**Institutional Review Board Statement:** Not applicable.

**Informed Consent Statement:** Not applicable.

**Data Availability Statement:** Data presented in this article is available on request from the corresponding author.

**Conflicts of Interest:** The authors declare no conflicts of interest.

## References

1. Tokuşlu, A. Analyzing the Energy Efficiency Design Index (EEDI) Performance of a Container Ship. *Int. J. Environ. Geoinf.* **2020**, *7*, 114–119. [CrossRef]
2. IMO. MEPC 80 highlights. In Proceedings of the 80th Session of the Marine Environment Protection Committee, MEPC 80, London, UK, 3–7 July 2023.
3. MEPC. *Guidelines on the Method of Calculation of the Attained Energy Efficiency Design Index (EEDI) for New Ships*; Circ: Danville, VA, USA, 2012; Volume 212, p. 1.
4. MEPC 59/Circ. 684. *Guidelines for Voluntary Use of the Ship Energy Efficiency Operational Indicator (EEDI)*; IMO: London, UK, 2009.
5. Ivanova, G. Analysis of the Specifics in Calculating the Index of Existing Marine Energy Efficiency EEXI in Force Since 2023. In Proceedings of the 13th Electrical Engineering Faculty Conference (BulEF), Varna, Bulgaria, 8–11 September 2021; Volume 2021, pp. 1–4. [CrossRef]
6. Introduction of EEXI, Korean Register. Available online: [https://www.krs.co.kr/kor/Content/CF\\_View.aspx?MRID=234&URID=72](https://www.krs.co.kr/kor/Content/CF_View.aspx?MRID=234&URID=72) (accessed on 11 January 2023).
7. Baldi, F.; Ahlgren, F.; Melino, F.; Gabriellini, C.; Andersson, K. Optimal load allocation of complex ship power plants. *Energy Convers. Manag.* **2016**, *124*, 344–356. [CrossRef]
8. Burt, C.M.; Piao, X.; Gaudi, F.; Busch, B.; Taufik, N.F. Electric motor efficiency under variable frequencies and loads. *J. Irrig. Drain. Eng.* **2008**, *134*, 129–136. [CrossRef]
9. IEA (International Energy Agency). Fuel Efficiency Labelling System. Available online: <https://www.iea.org/policies/980-fuel-efficiency-labelling-system> (accessed on 2 March 2023).
10. EPA (United States Environmental Protection Agency). EPA Federal Test Procedure. Available online: <https://www.epa.gov/emission-standards-reference-guide/epa-federal-test-procedure-ftp> (accessed on 3 March 2023).
11. DieselNet. Emission Test Cycles—FTP-75. Available online: <https://dieselnet.com/standards/cycles/ftp75.php> (accessed on 5 September 2023).
12. United States Environmental Protection Agency (US EPA). Dynamometer Drive Schedules. Available online: <https://www.epa.gov/vehicle-and-fuel-emissions-testing/dynamometer-drive-schedules> (accessed on 22 November 2023).
13. Fuel Efficiency and Grade Level in Automobiles, Korea Energy Agency. Available online: [https://bpms.kemco.or.kr:444/transport\\_2012/system/carlabel.aspx](https://bpms.kemco.or.kr:444/transport_2012/system/carlabel.aspx) (accessed on 23 November 2023).
14. Kruse, R.E.; Huls, T.A. *Development of the Federal Urban Driving Schedule*; Technical Paper 730553; SAE International: Warrendale, PA, USA, 1973. [CrossRef]
15. Karabasoglu, O.; Michalek, J. Influence of Driving Patterns on Life Cycle Cost and Emissions of Hybrid and Plug-In Electric Vehicle Powertrains. *Energy Policy* **2013**, *60*, 445–461. [CrossRef]
16. Öztürk, B. Energy Consumption and Emissions Characterization from Several Vehicle Technologies Considering Different Usage Profiles. Ph.D. Thesis, Técnico Lisboa, Lisbon, Portugal, 2013.
17. Choi, N.W.; Han, D.S.; Cho, S.W.; Cho, S.L.; Yang, J.S.; Kim, K.S.; Chang, Y.J.; Jeon, C.H. Development of a Vehicle Driving Cycle in a Military Operation Area Based on the Driving Pattern. *Trans. KSAE* **2012**, *20*, 60–67. [CrossRef]
18. Kyu-seong, W. Development of Tractor Driving Cycle for Fuel Economy Test on Chassis Dynamometer. Master's Thesis, Ajou University, Suwon, Republic of Korea, 2013.
19. Peng, J.; Jiang, J.; Ding, F.; Tan, H. Development of Driving Cycle Construction for Hybrid Electric Bus: A Case Study in Zhengzhou, China. *Sustainability* **2020**, *12*, 7188. [CrossRef]
20. Fotouhi, A.; Montazeri-Gh, M. Tehran Driving Cycle Development Using the k-Means Clustering Method. *Sci. Iran.* **2013**, *20*, 286–293.
21. Hung, W.-T.; Tam, K.-M.; Lee, C.-P.; Chan, L.-Y.; Cheung, C.-S. Comparison of Driving Characteristics in Cities of Pearl River Delta, China. *Atmos. Environ.* **2005**, *39*, 615–625. [CrossRef]
22. Moon, C.-J.; Roh, G.-T.; Kim, K.-W.; Park, K.-D. Preliminary Study on the Development of Sailing Modes for Ships. *J. Korean Soc. Mar. Eng.* **2023**, *47*, 275–284. [CrossRef]
23. Lee, T.C.; Judge, G.G.; Zellner, A. *Estimating the Parameters of the Markov Probability Model from Aggregate Time Series*. Data; North-Holland Publishing Company: Amsterdam, The Netherlands; London, UK, 1970.
24. Lee, Y.-K. Development of Driving Cycle for Fuel Consumption Measurement on the Basis of Proving Ground. Master's Thesis, Busan University, Busan, Republic of Korea, 2015.
25. Watson, H.C.; Milkins, E.E.; Braunsteins, J. The Development of the Melbourne Peak Cycle. In Proceedings of the SAE/ARRB 2nd Conference on Traffic Energy and Emissions, Melbourne, Australia, 19–21 May 1982.
26. Gammariello, R.T.; Long, J.R. Development of Unified Correction Cycles. In Proceedings of the Sixth CRC On-Road Vehicle Emissions Workshop, San Diego, CA, USA, 18–20 March 1996.

27. Dai, Z. *Driving Cycles: A New Cycle-Building Method That Better Represents Real-World Emissions*; Department of Civil & Environmental Engineering, University of California: Berkeley, CA, USA, 2008.
28. Sileghem, L.; Bosteels, D.; May, J.; Favre, C.; Verhelst, S. Analysis of Vehicle Emission Measurements on the New WLTC, the NEDC and the CADC. *Transp. Res. D* **2014**, *32*, 70–85. [[CrossRef](#)]
29. Korea Maritime and Ocean University. Introduction of the Ship Hannara. Available online: <https://www.kmou.ac.kr/stc/cm/cntnts/cntntsView.do?mi=4047&cntntsId=2621> (accessed on 10 December 2023).
30. Barceló, J.A. Chi-Square Analysis. In *The Encyclopedia of Archaeological Sciences*; Lopez, S.L., Ed.; John Wiley & Sons, Inc.: Hoboken, NJ, USA, 2018.

**Disclaimer/Publisher’s Note:** The statements, opinions and data contained in all publications are solely those of the individual author(s) and contributor(s) and not of MDPI and/or the editor(s). MDPI and/or the editor(s) disclaim responsibility for any injury to people or property resulting from any ideas, methods, instructions or products referred to in the content.